Automated Interference Lithography Systems for Generation of Sub-Micron Feature Size Patterns

Douglas S. Hobbs, Bruce D. MacLeod[*], Adam F. Kelsey, Mark A. Leclerc, Ernie Sabatino III, Daniel P. Resler

Holographic Lithography Systems (HLS), 3 Preston Court, Bedford, MA, 01730

ABSTRACT

Interferometric lithography is a maturing technology for patterning sub-micron structures in arrays covering large areas. The interference of two or more coherent optical waves is recorded in photoresist to produce a variety of structures including gratings, holes, posts, cones, and grids. This lithographic technique allows maskless patterning of large area substrates using short exposure times. Applications for periodic patterns include distributed feedback (DFB) lasers, field emission displays (FED), liquid crystal displays (LCD), advanced data storage applications, optical gratings, metrology standards, and motheye or sub-wavelength structures (SWS). Our work is motivated by interest in bringing interferometric patterning out of research laboratories and into mainstream production facilities where high volume applications require automation and simplification of the exposure process. The concept and operational principles of two automated interference lithography systems, the HLS System 1000, and the HLS Model PC2, are introduced.

Keywords: interference lithography, holographic, gratings, DFB, FED, LCD, photoresist, metrology, motheye, AR coating

1. INTRODUCTION

Interference (IL) or holographic lithography has been developed over the last 30 years with contributions by many researchers[1-11]. It is the preferred technique for patterning large area, nanoscale periodic features. Interference lithography is inherently maskless, with the optical beams interfering in a three dimensional volume, resulting in the capability to pattern non-flat surfaces. Typical interference configurations employ a method for splitting and expanding multiple coherent optical beams, and interfering the beams in the plane of a substrate coated with a photosensitive material. For a symmetric two-beam configuration, the relationship between grating period (Λ), laser wavelength (λ), incident beam angle (θ), and exposure medium (n) is well known.

$$\Lambda = \lambda / (2n\sin\theta) \tag{1}$$

The direct relationship between period and exposure wavelength has driven researchers to explore short wavelength laser sources to obtain the finest grating periods possible. The 351 nm line from an Argon ion laser has been commonly used to pattern structures as small 80 nm. One type of optical setup employs a folding mirror or prism to obtain interference from a single laser beam[1]. A more common configuration employs a beam splitter, mirrors, and spatial filters to direct two exposure beams onto the substrate[2-3]. This configuration can produce high fidelity patterns but has some inherent operational limitations. The optical train is relatively complex and is difficult and time consuming to reset for different period patterns. In addition, for periods less than 250 nm, UV laser sources are typically employed, which presents alignment difficulties and creates safety issues in a production environment.
The pattern geometries described in this paper can also be defined by other exposure techniques, including e-beam writing, phase masks, high precision steppers, and other emerging technologies. However, each technique has its own inherent drawbacks and considerations including system cost, field size, depth of focus, and patterning speed.

2. INTERFERENCE LITHOGRAPHY

2.1 Multiple Beam Interference

Coherent addition of two plane waves produces an aerial image in the form of a one dimensional sinusoidal intensity distribution. The coherent addition of three or more plane waves results in a redistribution of energy into regions where

constructive interference occurs. The result is an increased image intensity gradient, while requiring less energy per incident beam. A mathematical representation of the intensity distribution formed by coherent interfering plane waves is given by

$$I= |\Sigma_N \mathbf{E}_N|^2 \quad (2)$$

where $\mathbf{E}_N$, the electric field vector describing the Nth plane wave, is given by

$$\mathbf{E}_N= \mathbf{A}_N \exp[i(\mathbf{k}_N.\mathbf{r}_N-\omega t)]. \quad (3)$$

In equation 3, $\mathbf{A}_N$ is a vector describing the amplitude and polarization of the Nth plane wave, $\mathbf{k}_N$ and $\mathbf{r}_N$ are the wave vector and position vector of the Nth plane wave, ω is the angular frequency and t is time. The pertinent mathematical model for each of these cases is described below.

2.2.1 Two Beam Interference

Two beam interference produces an intensity modulation in only one direction. It is assumed that two coherent plane waves are propagating in air with k vectors in the x-z plane incident onto the x-y plane at symmetric angles, +/- ϕ, with respect to the z axis. The equation for the resulting intensity distribution is given by

$$I= 2A^2[1+\cos(2kx\sin\phi)], \quad (4)$$

where λ is the wavelength in air, $k = 2\pi/\lambda$, and the plane waves have equal amplitude, A. This two beam intensity distribution is constant along the y-axis while varying sinusoidally in the x-z plane with a period $\Lambda= \lambda/2\sin\phi$. The maximum intensity, $I_{max}= 4A^2$, occurs when the modulation term is equal to 1 while the minimum intensity, $I_{min}= 0$, occurs when the modulation term is equal to 0. Note that maximum intensity contrast occurs only when the two beams have equal amplitudes.

2.2.2 Crossed Two Beam Interference

In a crossed two-beam exposure, the intensity distribution from orthogonal two beam exposures are superimposed. It is assumed that the substrate is exposed to two coherent plane waves propagating with k vectors in the x-z plane, the same as for the two-beam case above. The substrate is then rotated 90°, and re-exposed with plane waves propagating with k vectors in the y-z plane (with respect to the substrate coordinate system), at symmetric angles +/- ϕ with respect to the z axis. The equation for the resulting intensity distribution (assuming equal plane wave amplitudes) is given by

$$I= 2A^2[2+\cos(2kx\sin\phi)+ \cos(2ky\sin\phi)]. \quad (5)$$

A contour plot of the crossed two beam intensity distribution is shown in Figure 1. A square array is formed having maxima spaced at identical periods of $\Lambda= \lambda/2\sin\phi$ along the x and y axes. The maximum intensity $I_{max}= 8A^2$ occurs when the intensity maxima of the two fringe patterns overlap. The minimum intensity $I_{min}= 0$ occurs when the intensity minima of the two fringe patterns overlap. The intermediate intensity $I_{int}=4A^2$ occurs when the intensity maximum of one fringe pattern overlaps the intensity minimum of the other. The individual beam intensity should be reduced from the two-beam interference case due to the additive nature of the crossed two-beam exposure.

2.2.3 Three Beam Interference

Coherent addition of three beams in a symmetric configuration results in an intensity distribution with modulation in three directions forming peaks on a close-packed hexagonal grid. The three coherent plane waves are assumed to originate from point sources located at the corners of an equilateral triangle in the x,y,z plane at a height z = h above the exposure plane. The beams are thus 2θ = 120 degrees apart in the x,y plane and tilted at an angle ϕ with respect to the z-axis. The equation for the resulting intensity distribution (assuming equal plane wave amplitudes) is given by

$$I = 3A^2+2A^2\cos(kx\sin\theta\sin\phi+ky\sin\phi[1+\cos\theta])+2A^2\cos(-kx\sin\theta\sin\phi+ky\sin\phi[1+\cos\theta])+ 2A^2\cos(2kx\sin\theta\sin\phi). \quad (6)$$

The coherent summation of the three beams produces a hexagonal array with an intensity peak located at the center of each hexagon. The period between the central peaks is equal to $(2/3^{1/2})d$, where $d= \lambda/2\sin\psi$ is the fringe spacing between any beam pair and ψ is the half angle between beams.

Figure 2 shows a contour plot of the intensity distribution given in equation 6 depicting hexagonally shaped intensity maximum surrounded by smaller triangles. According to reference 2, the triangles are zero intensity points with $I_{min}= 0$. Each intensity maximum, $I_{max}= 9A^2$, is surrounded by an area of intermediate intensity, $I_{int}= A^2$, forming a saddle point between each zero intensity point. The ratio of intensity peak to the intermediate intensity at the saddle point is 9:1. Three-beam interference produces larger intensity gradients (sharper peaks) than crossed two-beam interference.

2.2.4 Four Beam Interference

Simultaneous four beam interference produces intensity peaks on a rectangular grid. Four coherent plane waves are assumed to originate from point sources located at the midpoint of each side of a square (forming a cross pattern) in the x,y,z plane at a height z = h above the exposure plane. The plane waves are thus $2\theta= 90$ degrees apart in the x,y plane and tilted at an angle ϕ with respect to the z-axis. The equation for the resulting intensity distribution (assuming equal plane wave amplitudes) is given by

$$I= 2A^2[2+\cos(2ky\sin\phi)+\cos^2\phi\cos(2kx\sin\phi)-\sin^2\phi\cos(2kx\sin\phi)+4\cos\phi\cos(kx\sin\phi)\cos(ky\sin\phi)]. \quad (7)$$

It has been previously shown[4] that in the small angle approximation for ϕ, equation 7 reduces to

$$I= 2A^2[2+\cos(2ky\phi)+\cos(2kx\phi)+4\cos(kx\phi)\cos(ky\phi)], \quad (8)$$

where the last term of equation 8 has a period that is twice that of the first two terms. This term cancels alternate rows and columns of intensity maximum produced by the constructive interference of the first two terms, while maintaining the face centered cubic position. The result is a square array of intensity maximum rotated 45 degrees and having a period $\Lambda=\lambda/2^{1/2}\sin\phi$, $2^{1/2}$ times larger than for crossed two beam interference at the same angles ϕ.

A contour plot of the intensity distribution given in equation 8, shown in Figure 3, depicts square shaped intensity maximum. From equation 8, $I_{max}= 16$ when all the fringe patterns add in phase. Each square shaped intensity maximum is surrounded by a line of minimum intensity $I_{min}= 0$, which occurs when all the fringe patterns add out of phase, giving a very large intensity gradient. The four-beam exposure has the advantage of large contrast at the expense of more complex setup and alignment of the additional exposure beams. Also, careful beam alignment is required to prevent generation of a Moiré pattern across the exposure plane.

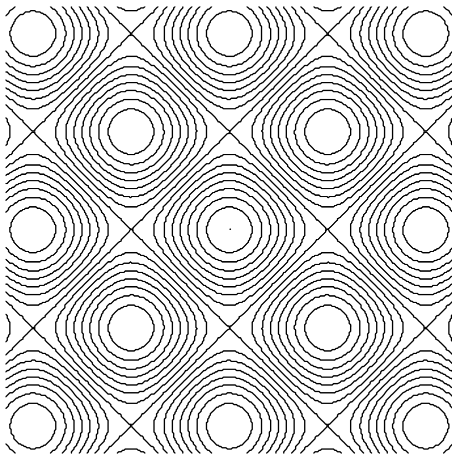

Fig. 1 Intensity distribution of crossed two beam interference exposure.

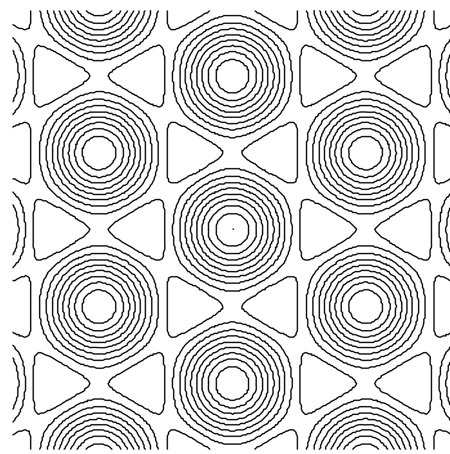

Fig. 2 Intensity distribution of three beam interference exposure.

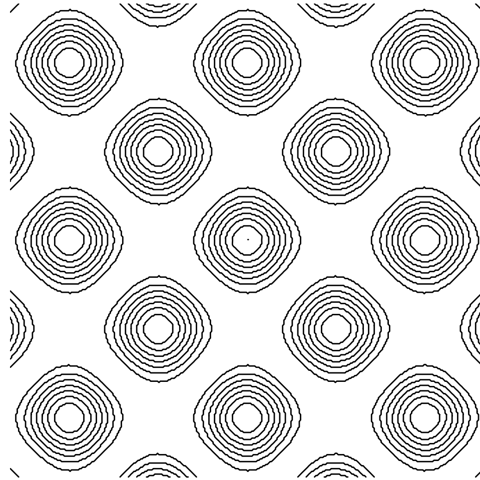

Fig. 3 Intensity distribution of four beam interference exposure with beams configured 90 degrees apart.

2.3 Conventional Experimental Configuration

Interference patterns are commonly generated in the laboratory on an isolation table using common optical components. A laser source emitting a polarized beam at a wavelength within the sensitivity range of available photosensitive media is employed. The source must also operate with a sufficiently large coherence length to facilitate patterning of large areas, and to provide tolerance in the setting of the relative path lengths traveled by the interfering beams. For many applications, photoresist is the photosensitive medium employed where the illumination source must have a wavelength in the UV or blue regions of the spectrum. Suitable gas laser sources include Krypton-ion (413.1nm), Argon-ion (351, 364.8, 457.9nm), and Helium-Cadmium (442.1nm). Referring to Figure 4, the laser beam is directed by mirrors through a series of beam splitters, which divide the source into multiple equal power beams – in this case three. The split beams are directed into spatial filters located such that the point sources generated by each filter lie in a plane parallel to the substrate plane. In the schematic shown in Figure 4, the three point sources are placed in a triangular configuration (the center beam is above the plane of the table) with their energy directed at the center of a recording plane. An interference pattern, such as that described in Section 2.2.3, is formed throughout the volume over which the three beams overlap. A wafer or glass panel coated with photoresist is then placed in the recording plane, exposed to the interference pattern, and developed.

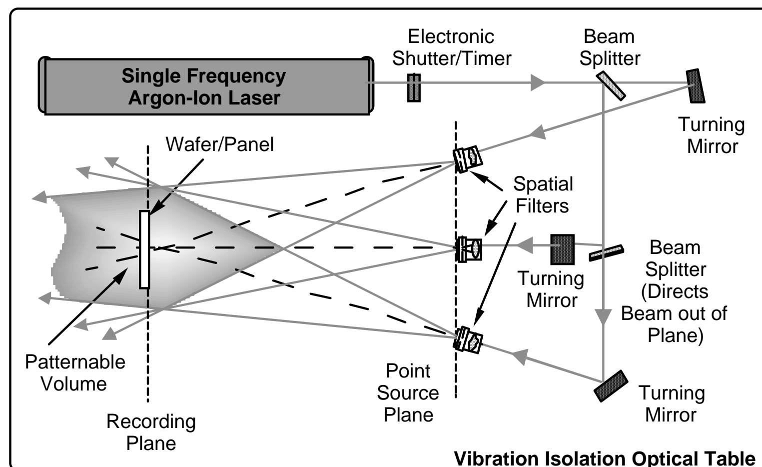

Fig. 4 Schematic of typical tabletop two beam interference lithography setup

3. AUTOMATED INTERFERENCE LITHOGRAPHY SYSTEM DESIGN PRINCIPLES

3.1 Fiber Delivery System for Blue Light

The primary advantage of the automated interference lithography systems described here is the ability to quickly and accurately change pattern period and shape. The enabling technology for our systems is that operation in the blue, at 457.9 nm, allows the use of fibers to control the optical path. Conventional IL tabletop systems utilize UV lasers where optical fiber performance and lifetime is inadequate. The automated IL systems described here efficiently couple light from an Argon ion laser into one or more fibers. The fiber outputs are rigidly mounted on motorized, optically encoded translation stages, which allow the operator to select the pattern pitch in an automated fashion. The fiber position can be changed in seconds with a high degree of repeatability determined by the optical encoders. By contrast, reconfiguration of a typical tabletop interference lithography setup can take hours using a highly skilled operator.

Photoresist sensitivity is typically lower in the blue than in the UV. However, the blue wavelength is a more practical choice for the automated IL production system. In addition to enabling the fiber delivery system as described above, the blue wavelength relieves some eye-safety concerns associated with a UV source. The visible wavelength source also simplifies system optical alignment, maintenance and troubleshooting.

3.2 Automation

The HLS IL systems employ a fully automated Labview software user interface, which requires only minimum operator involvement in the system configuration, calibration and exposure routines.

3.2.1 Pitch Selection

The fiber outputs are mounted on piezo-driven rotary stages, which are attached to carriages riding on a linear rail system. A linear servo motor drives the carriage with positional feedback from an optical encoder. A home position along the rail is established with repeatability of a few microns. A custom designed braking mechanism locks the carriage to the rail with no power supplied to the brake. This is extremely important during the exposure process where mechanical stability is critical. The translational resolution of the fiber output is on the order of 10 um, which corresponds to a pattern pitch resolution of fractions of an angstrom in our current system configuration. The operator can select a target pitch by typing the desired pitch into a data input box within the LabView user-interface. There is also an option to move the fiber outputs to an absolute user defined position.

3.2.2 System Calibration

System calibration is achieved through real-time feedback from a CCD camera. A CCD camera mounted above the exposure plane images the intensity distribution of each exposure beam. Camera feedback enables automated centering, power balance, fiber input coupling and dose calibrations for each exposure beam. The system calibration routine takes about 15 minutes with a new pitch selection. Calibration is not generally required for successive exposures at the same pitch.

3.2.3 Beam Center Calibration

Once the fiber outputs are at the desired location, the first calibration is to center the exposure beams on the wafer chuck. A peak finding routine locates the peak of the gaussian beam. A signal proportional to the distance between the intensity peak and the wafer chuck center is sent to the fiber output rotation stage, which centers the peak within a few iterations. The shutter for each exposure beam is opened sequentially and the beam centering calibration is repeated.

3.2.4 Fiber Input Coupling Calibration

Once the beams are centered, the coupling of light into each fiber input is optimized. The fiber inputs are mounted to multi-axis stages, which are driven through piezo motors. A tuning sequence is performed moving the axes of each fiber input through a defined sample space using the peak intensity imaged by the camera as feedback. The mechanical stability of the

automated IL systems is such that from day to day only slight adjustments of the fiber input are necessary to maximize coupling.

3.2.5 Fiber Output Power Balance

After centering the exposure beams and maximizing the optical input coupling, the fiber output powers are balanced. This calibration is very important because a power imbalance leads to contrast reduction in the interference pattern. The peak intensity of each exposure beam is measured with the CCD camera. A signal related to the difference in peak beam intensities is sent to a variable beam splitter in the input coupling subsystem located between the laser and the fiber inputs. The beam-split ratio is adjusted until the beam powers are equal.

3.2.6 Dose Calibration

As the fiber positions are changed to pattern smaller pitches, the distance between the fiber output and exposure plane increases, reducing the beam intensity at the exposure plane. To maintain a target exposure dose, the exposure time is subsequently increased for smaller pitches. A response curve is generated for the HLS IL system, which correlates CCD pixel value to beam intensity at the exposure plane over the entire range of available pitches. We can therefore determine the required exposure time to achieve the target dose. The dose calibration is fully automated within the LabView user-interface.

3.2.7 Run Job

Once the system has been calibrated, the operator can expose a wafer by selecting a job from a job database. A job consists of a job name, grating pitch, and exposure dose. The operator is prompted to load a wafer on the wafer chuck. The job then continues by moving the wafer chuck to the expose position. Fiber shutters are opened for the time corresponding to the target dose and measured beam intensity. The fiber shutters close after exposure and the wafer is returned to the load position. The entire exposure sequence is hands-free and the automated exposure parameters ensure pattern uniformity and repeatability wafer to wafer.

4. SYSTEM 1000 EXPOSURE SYSTEM

The HLS System 1000 exposure system can be configured with two, three, four, or more optical beams. In practice, two and three beam exposures appear to have the most promising applications. The beam delivery system is fully automated and utilizes the Argon ion laser as described above. The exposure process is compatible with commercially available production g-line photoresists and developers, such as the AZ Clariant 1500 photoresist series.

4.1 Two beam interference exposures

High fidelity two beam exposures have been demonstrated with pattern periods from 0.28 to 4 microns. Maximum interference exposure doses of 120-200 mJ, corresponding to exposure times from 30 seconds to over a minute are required. The specific dose is defined by the desired pattern pitch, photoresist thickness, and developer normality. The contrast of the exposure and development process can be exploited to control pattern profile. High contrast processes have been demonstrated to obtain 4:1 aspect ratio patterns, as shown in the scanning electron micrograph (SEM) of Figure 5. These patterns are ideal as etch masks for reactive ion etching and micro-machining applications. Samples sizes up to 5” diameter have been demonstrated. Conversely, lowering the process contrast can give the desired effect of directly recording the sinusoidal interference pattern. This analog pattern is often desired in high efficiency optical grating applications and is shown in figure 6.

4.2 Crossed two beam interference exposures

By rotating the sample wafer by 90 degrees for a second exposure, a post or hole pattern can be obtained. The resultant pattern shape is dependent on a number of parameters, including exposure dose, developer normality, and development time.

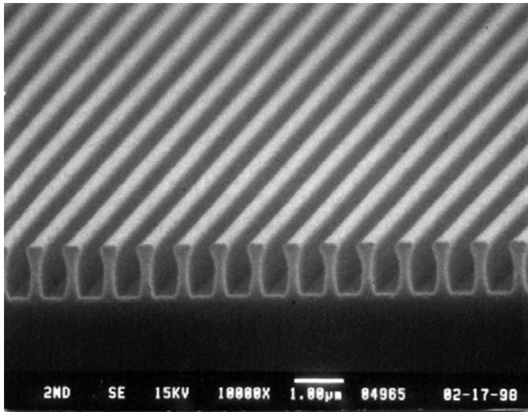

Fig. 5 SEM of high contrast two beam interferometric process. Pattern period is 800 nm, with a feature aspect ratio of 4:1.

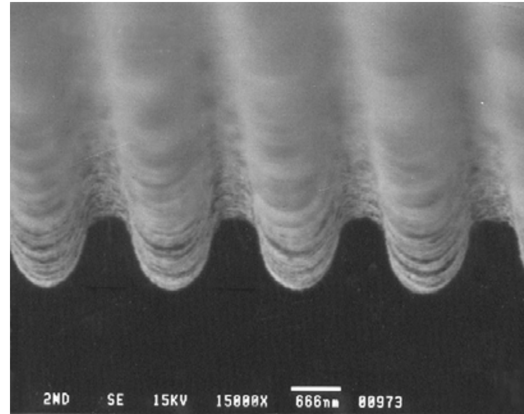

Fig. 6 SEM of low contrast process for two beam interferometric exposure. Pattern period is 1.6 microns.

4.2.1 "Motheye" antireflection surfaces

The crossed two beam exposure technique has been exploited to pattern "motheye" antireflection surfaces for the visible and infrared spectral regions[6]. Figure 7 demonstrates a photoresist motheye structure recorded for visible antireflection applications. The photoresist pattern is used as a master for high volume replication of visible antireflection products. The textured photoresist surface is also often used as an etch mask for transferring the motheye directly into the substrate material. Figure 8 shows a motheye surface etched into silicon for midwave infrared (MWIR) antireflection applications. The motheye surface texture acts to gradually grade the refractive index of the substrate material to the refractive index of air, effectively suppressing surface reflections[13,14]. As a result of the large depth of focus for IL patterning, the technique is especially effective in patterning motheye on curved surfaces, such as lenses and custom optics.

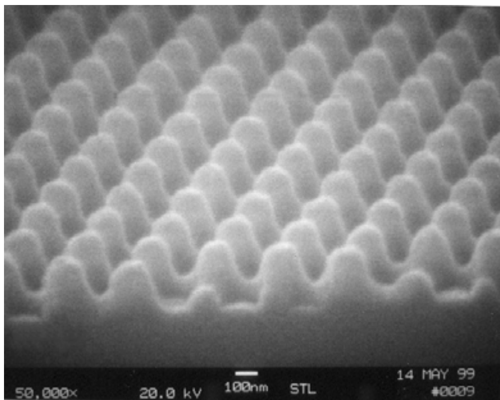

Fig. 7 SEM micrograph of crossed two beam interferometric exposure for fabrication of motheye anti-reflection surface. Pattern period is 280 nm.

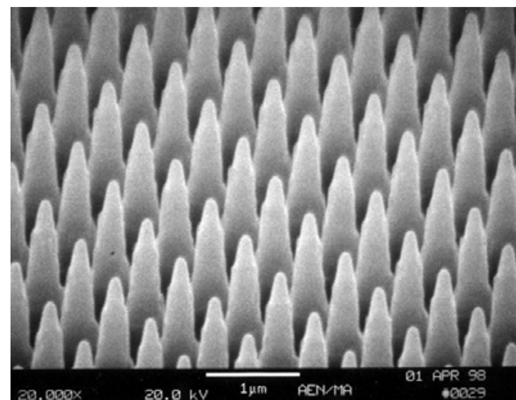

Fig. 8 SEM micrograph of etched silicon motheye surface for MWIR antireflection applications. Motheye depth is 2.0 microns.

4.3 Three beam interference exposures

The HLS System 1000 is easily reconfigured for three beam exposures. The laser source is split into three beams of equal intensity and the fiber outputs are typically placed concentrically 120 degrees apart above the wafer plane. The intensity

profile obtained by the coherent summation of the three beams produces extremely high fidelity hole or dot patterns. The process contrast has been exploited to produce high aspect ratio hole patterns over areas as large as 5” diameter. Hole diameters from 400 nm to 3.0 microns have been demonstrated. Figure 9 shows a SEM micrograph of 500 nm diameter holes patterned on a 1.2 micron period, while figure 10 shows 1.4 micron diameter holes on a 2.4 micron hexagonal period. For the 1.4 micron hole pattern, hole diameter variation across a five inch diagonal field has been measured to be less than 5% via SEM analysis with sidewall angles greater than 80 degrees.

4.3.1 Field Emission Display (FED) applications

Periodic hole patterns are ideal for field emission display applications (FED), where lithography is typically employed to define holes for the Spindt emitter tip fabrication process[12]. The photoresist pattern is used as a mask during a dry etch process to transfer the hole pattern into underlying thin film layers. Emitter tips are then deposited within the holes with off-axis evaporation techniques. Decreasing the emitter hole diameter and increasing density of emitter tips has been shown to result in lower power requirements and higher reliability of field emission devices[7-11]. To define holes in the FED fabrication process, manufacturers typically employ steppers, which have field size, throughput, and stitching issues. Interference lithography offers small feature size patterns over large fields, with relative short exposure times.

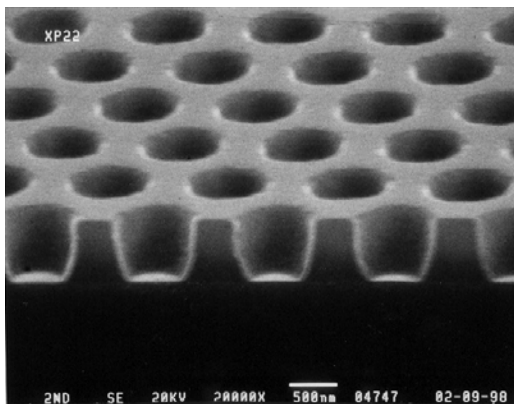

Fig. 9 SEM micrograph of high contrast three beam interferometric exposure. Hole diameter is 500 nm on a 1.2 micron hexagonal period grid.

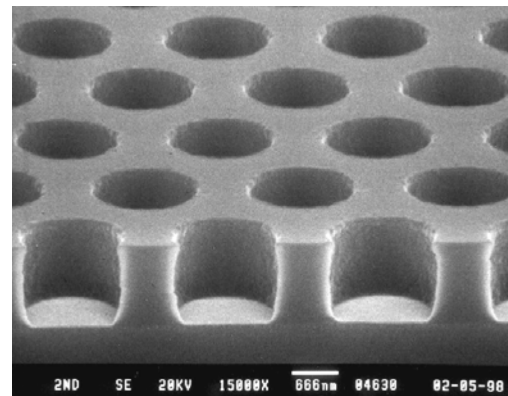

Fig. 10 SEM micrograph of high contrast three beam interferometric exposure. Hole diameter is 1.4 microns on a 2.4 micron hexagonal period grid.

4.3.2 Liquid Crystal Display (LCD) alignment layer applications

A major advantage of using our fiber optic beam delivery system is the ability to configure multiple beams arbitrarily and asymmetrically. Three beams can be configured to create asymmetric, or blazed gratings, which have potential use in LCD alignment layer applications. Bistable surface alignment has been demonstrated for Zenithal Bistable Device (ZBD) liquid crystal displays. Gratings have also been fabricated to allow voltage controlled twists (VCT) in VCT LCDs.

4.3.3 Asymmetric patterns

The inherent flexibility of the fiber delivery system allows the operator to configure the exposure beams arbitrarily. One configuration places the exposure beams at the corners of a right triangle, which produces an oval pattern in photoresist, as shown in figure 11. Asymmetric patterns could have applications for fabricating polarizing or birefringent optics. For a two beam configuration, setting the beams with differing incident angles and/or heights with respect to the recording plane will result in a grating period variation or “chirp” across the substrate. Chirped gratings are desirable in many spectroscopy applications.

4.4 Four or more beam interference exposures

In addition, four or more beams can be used to obtain complex pattern geometries with very short exposure times. Figure 12 demonstrates a 900 nm period grid pattern exposed with four coherent beams configured at the corners of a square centered above the substrate, in a plane parallel to the substrate plane. However, Moiré patterns generated with the redundant beam pairs must be handled according to the requirements of each application.

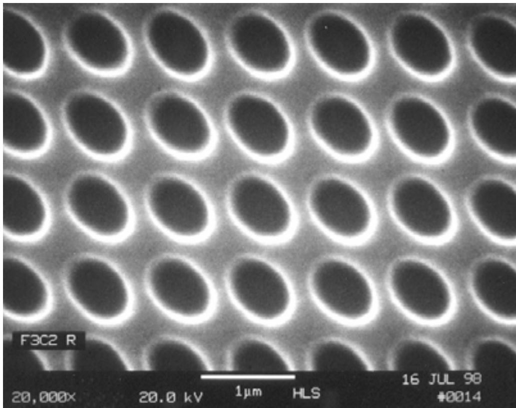

Fig. 11 SEM micrograph of high contrast three beam interferometric exposure with beams aligned in right triangle configuration. Pattern period is 850 nm.

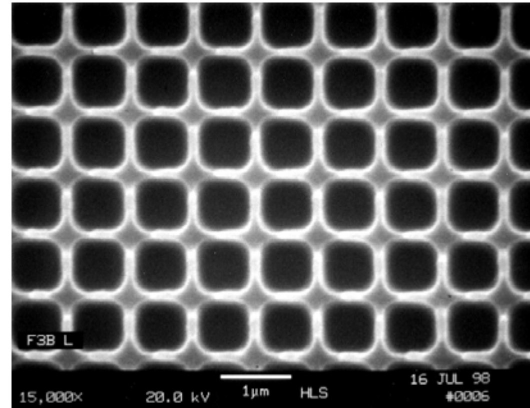

Fig. 12 SEM micrograph of high contrast four beam exposure "grid" pattern. Grid period is 900 nm.

5. MODEL PC2 EXPOSURE SYSTEM

The HLS model PC2, schematically illustrated in Figure 13, is a two-beam interferometric pattering tool designed to pattern features with dimensions as small as 80 nm. Like the system 1000, the fiber optic delivery system is fully automated and computer controlled, and employs an Argon ion laser operating at 458 nm. However, to reach extremely fine pitch patterns, the technique of optical prism coupling is applied. The fundamental lower limit of pattern period in air is described by $\lambda / (2n \sin\theta)$ with $n = 1$. In practice, using blue light, this limits air exposure patterns to periods greater than 260 nm. However, the model PC2 exposure tool exploits the refractive index parameter in the grating equation. By using an exposure prism, the index of the incident medium is increased to about 1.5, effectively compressing the pattern pitch by the same factor. To provide optical coupling into the photoresist layer, a fluid is inserted between the wafer and prism prior to exposure. The fluid is removed at the completion of exposure. Shank and Schmidt describe this exposure technique in a previous work[15]. For a typical exposure dose of 120 mJ, exposure times fall into the range of 25-40 seconds. The system technician controls the automated exposure sequence through the screen monitor, and is required to load and unload wafers. Patterns as fine as 190 nm period and 80 nm critical dimension have been repeatedly demonstrated with commercially available g-line photoresists and developers. Figure 14 shows the model PC2 automated IL system.

5.1 Distributed feedback laser (DFB) fabrication

The PC2 system is ideal for patterning 2"-3" diameter wafers with grating periods of 190-260 nm. One major application of patterning fine pitch gratings is in distributed feedback laser (DFB) fabrication. DFB lasers are used extensively as single frequency light sources for fiber optic telecommunications. The DFB laser structure requires a high fidelity etched grating across a two or three inch InP wafer to define the laser wavelength. The photoresist grating is used as an etch mask for subsequent reactive ion etching of the active epitaxial layers. The two principle operational wavelength regions for fiber based telecommunications are 1290-1330 nm and 1520-1580 nm, corresponding respectively to 199-206 nm and 235-245 nm grating periods in the DFB laser. Figures 15 and 16 show nominal 200 nm and 240 nm period photoresist grating cross-sections with greater than a 1:1 feature aspect ratio. The uniform, straight sidewall photoresist patterns with a nominal 55/45 mark/space ratio are ideal etch masks for high yield DFB laser fabrication.

Of significant concern to DFB laser manufacturers is the specification of pitch accuracy and pitch variation across a single wafer. DFB lasers operate at discrete wavelengths, with “dead bandwidth” between operational wavelengths. The PC2 pitch variation specification for a 2” diameter wafer is less than .04 A/mm variation in the 200 nm period region and .07A/mm variation in the 240 nm period region. This falls well within current manufacturing specification for DFB laser fabrication.

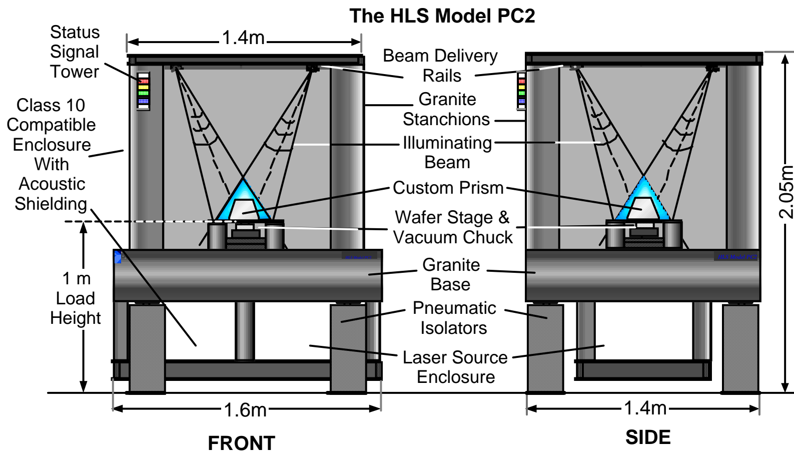

Fig. 13 Front and side illustrations of model PC2 IL system.

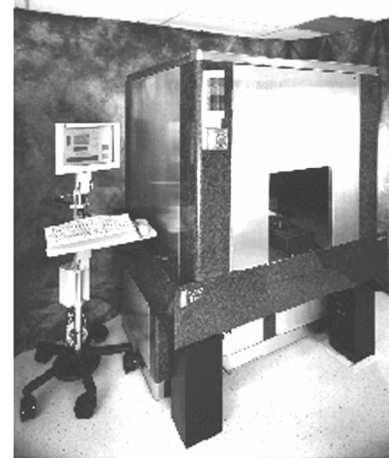

Fig. 14 PC2 automated interference lithography system for patterning 190 nm to 4 micron period patterns

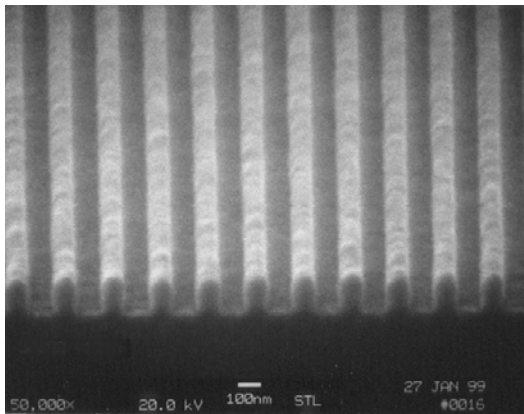

Fig. 15 High aspect ratio 200 nm grating patterned on a 2” InP wafer for DFB laser fabrication

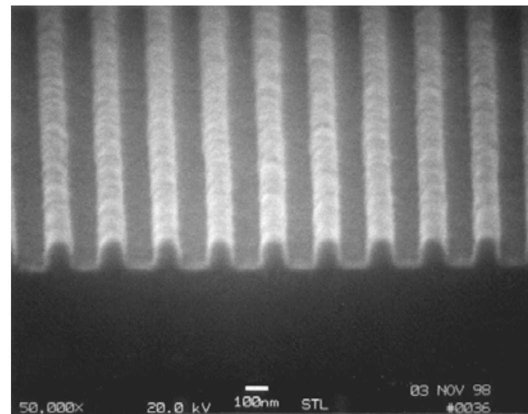

Fig. 16 High aspect ratio 240 nm grating patterned on a 2” InP wafer for DFB laser fabrication

5.2 High density data storage applications

The automated wafer chuck assembly on the PC2 readily allows for multiple rotational exposures on a single wafer, such as the crossed two-beam pattern. As described in section 2.2.2, this exposure sequence results in a hole or post pattern on a square grid. A promising application for this type of pattern is in high density memory applications, where there is a continual push towards increasing disk-drive capacity. Figure 17 demonstrates a post pattern with a 193 nm period, which defines a density of 17.3 billion dots per square inch.

5.3 Metrology standards

The precision of the PC2 beam delivery system is also ideal for fabricating high accuracy, high contrast metrology standards for SEM, AFM, and optical applications. As required for DFB laser fabrication, the system PC2 patterns grating periods to an absolute accuracy of better than 1 angstrom relative to a specified standard. Figure 18 demonstrates a 200.0 nm period metrology standard on a silicon substrate.

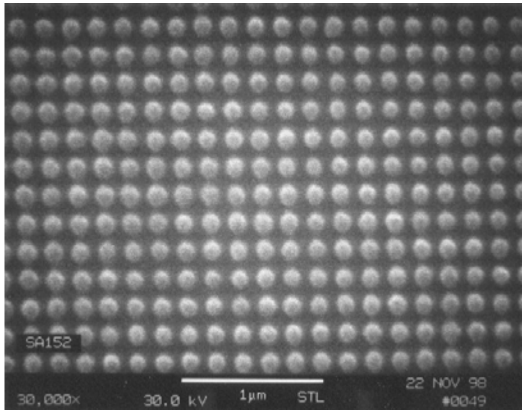

Fig. 17 193 nm period posts patterned on a 3" diameter silicon wafer for high density data storage applications

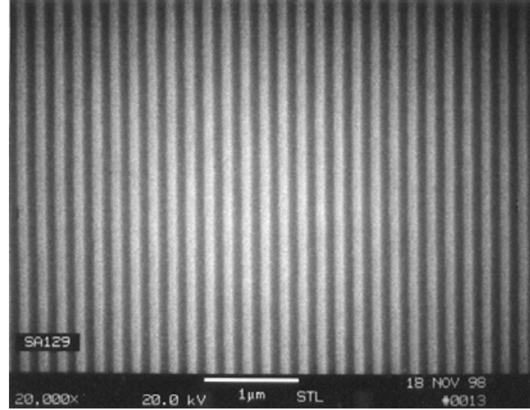

Fig. 18 200.0 nm period grating fabricated for calibration and metrology applications

6. SUMMARY

We have introduced the first fully automated interference lithography based exposure systems. The utilization of fiber optic technology and mechanical automation has demonstrated the ability to quickly and accurately change pattern period and shape. Operation with the relatively eye-safe 458 nm Argon ion laser light enables the use of the fiber optic beam delivery system. The use of a visible light exposure source also simplifies system alignment, calibration, and maintenance. Patterning processes and results, based on the use of production proven g-line positive photoresist products, have been demonstrated for applications requiring high speed, large area, high fidelity patterning. In addition, the inherent flexibility of the multiple beam configurations allows for exploring custom optical patterns, such as chirped gratings, asymmetric structures, and sub-wavelength structures.

ACKNOWLEDGEMENTS

The authors would like to thank Greg Sonek for technical assistance in preparing the manuscript, and John Knowles for timely assistance with the SEM work.

REFERENCES

1 S. H. Zaidi and S. R. J. Brueck, "High aspect ratio holographic photoresist gratings", Appl. Opt. 27, no. 14, pp. 2999-3002, 1988.

2 J. J. Cowan, "The Recording and Large Scale Replication of Crossed Holographic Grating Arrays Using Multiple Beam Interferometry", Proc. SPIE, Vol 503, pp. 120-129, 1984.

3 M. L. Schattenberg, C.R. Canizares, D. Dewey, K.A. Flanagan, M.A. Hamnett, A.M. Levine, K. Lum, R. Manikkalingam, T.H. Markert, " Transmission grating spectroscopy and the advanced x-ray astrophysics facility", Optical Eng., vol. 30, no. 10, pp. 1590-1599, 1991.

4 S. H. Zaidi, S. R. J. Brueck, F. M. Schellenberg, R. S. MacKay, K. Uekert, and J. J. Persoff., "Interference Lithography Exposure Tool for 180-nm Structures". Proc. SPIE, Vol 3048, pp. 248-254, 1997.

5 M. L. Schattenberg, R. J. Aucoin, and R. C. Fleming, "Optically matched trilevel process for nanoscale fabrication", J. Vac. Sci. Tech., B13(6), pp.3007-3011, 1996.

6 S. J. Wilson and M. C. Hutley, "The optical properties of motheye antireflection surfaces", Optica Acta, vol. 29, no. 7, pp 993-1009, 1982.

7 C. O. Bozler, C. T. Harris, S. Rabe, D. D. Rathman, M. A. Hollis, H. I. Smith, "Arryas of gated field emitter cones having 0.32 micron tip to tip spacing", J. Vac. Sci. Tech. B12(2), pp. 629-632, 1994.

8 J. P. Spallas, A. M. Hawryluk, and D. R. Kania, "Field emitter array mask patterning using interference lithography", J. Vac. Sci. Tech. B13, pp. 1973-1978, 1995.

9 X. Chen, S. H. Zaidi, S. R. J. Brueck, and D. J. Devine, "Interferometric lithography of sub-micrometer sparse hole arrays for field-emission display applications", J. Vac. Sci. Tech. B 14, pp. 3339-3349, 1996.

10 A. Fernandez, J. Y. Decker, S. M. Herman, D. W. Phillion, D. W. Sweeney, and M. D. Perry, "Methods for fabricating array of holes using interference lithography", J. Vac. Sci. Tech. B 15(6), Nov/Dec, pp. 2439-2443, 1997.

11 A. Fernandez, H. T. Nguyen, J. A. Britten, R. D. Boyd, M. D. Perry, D. R. Kania, and A. M. Hawryluk, "The use of interference lithography to pattern arrays of submicron resist structures for field emission flat panel displays", J. Vac. Sci. Tech. B 15(3), pp. 729-735, 1997.

12 C. A. Spindt, C. E. Holland, A. Rosengreen, and I. Brodie, IEEE Trans. Electron Devices ED-38, pp. 2355, 1991.

13 D. H. Raguin and G. M. Morris, "Antireflection structured surfaces for the infrared spectral region", Applied Optics, vol. 32, No. 7, pp. 1154-1167, 1993.

14 W. H. Southwell, "Pyramid-array surface relief structures producing antireflection index matching on optical surfaces", J. Opt. Soc. Am. A, Vol. 8, No. 3, pp. 549-553, 1991.

15 C. V. Shank and R. V. Schmidt, Appl. Phys. Lett., Vol. 23, No. 3, pp. 154-155, 1973.

* Correspondence: Email: motheye@msn.com WWW: hlstech.com telephone: 781-276-0538 FAX: 781-276-4074